Dissolved greenhouse gases (nitrous oxide and methane) associated with the naturally iron-fertilized Kerguelen region (KEOPS 2 cruise) in the Southern Ocean

L. Farías[1]*, L. Florez-Leiva[2], V. Besoain[1,3], G. Sarthou[4], and C. Fernández[5]

[1] Departamento de Oceanografía. Universidad of Concepción and Centro de Ciencia del Clima y la Resiliencia (CR)[2], Chile

[2] Programa de Biología. Universidad del Magdalena, Santa Marta, Colombia

[3] Escuela de Ciencias del Mar, Pontificia Universidad Católica de Valparaíso, Chile

[4]LEMAR-UMR 6539, CNRS-UBO-IRD-IFREMER, Place Nicolas Copernic, 29280 Plouzané, France

[5]Sorbonne Universités, UPMC Univ Paris 06, UMR 7621, Laboratoire d'Océanographie Microbienne, Observatoire Océanologique, F-66650 Banyuls/mer, France and Department of Oceanography, COPAS SA program and Interdisciplinary Center for Aquaculture Research (INCAR), University of Concepción, Chile

Correspondence should be addressed to:

Laura Farias; lfarias @profc.udec.cl

ABSTRACT

The concentrations of greenhouse gases (GHGs), such as nitrous oxide (N_2O) and methane (CH_4), were measured in the Kerguelen Plateau Region (KPR). The KPR is affected by an annual microalgal bloom caused by natural iron fertilization, and this may stimulate the microbes involved in GHG cycling. This study was carried out during the KEOPS 2 cruise during the austral spring of 2011. Oceanographic variables, including N_2O and CH_4, were sampled (from surface to 500 m depth) in two transects along and across the KRP, the north-south (TNS) transect (46°-51°S, ~72°E) and the east-west (TEW) transect (66°-75°E, ~48.3°S); both associated with the presence of a plateau, Polar Front (PF) and other mesoscale features. The TEW presented N_2O levels ranging from equilibrium (105%) to slightly supersaturated (120%) with respect to the atmosphere whereas CH_4 levels fluctuated dramatically, being highly supersaturated (120-970%) in areas close to the coastal waters of Kerguelen Island and in the PF. The TNS showed a more homogenous distribution for both gases, with N_2O and CH_4 levels ranging from 88% to 171%, and 45% to 666% saturation, respectively. Surface CH_4 peaked at southeastern stations of the KPR (A3 stations) where a phytoplankton bloom was observed. Both gases responded significantly, but in contrasting ways (CH_4 accumulation and N_2O depletion), to the patchy distribution of chlorophyll a. This seems to be associated to the supply of iron from various sources. Air-sea fluxes for N_2O (from -10.5 to 8.65, mean 1.25±4.04 μmol m^{-2} d^{-1}) and for CH_4 (from 0.32 to 38.1, mean 10.01±9.97 μmol $^{-2}$ d^{-1}) indicated that the KPR is both a sink and a source for N_2O, and a considerable and variable source for CH_4. This appears to be associated with biological factors, as well as the transport of water masses enriched with Fe and CH_4 from the coastal area of the Kerguelen Islands. These previously unreported results for the Southern Ocean suggest an intense microbial CH_4 production in the study area.

Keywords: Nitrous oxide, methane, dissolved iron fertilized Kerguelen area, mesoscale structures and polar front Southern Ocean.

1. **Introduction**

The increasing concentration of greenhouse gases (GHGs) in the troposphere, such as CO_2, N_2O and CH_4, affect the Earth's radiative balance. Additionally, the increasing concentration of ozone-depleting gases (such as chlorofluorocarbons and N_2O) in the stratosphere is weakening the ozone shield, permitting higher levels of damaging ultraviolet radiation to reach the Earth's surface. The relative potency of a GHG is determined by its respective residence time in the atmosphere (Cicerone and Orelamland, 1988), and the extent of magnitude of emissions to the atmosphere, of which the input/contribution from the ocean is considered to be important (IPCC, 2013).

Although oceans are generally considered to be a net source of GHGs to the atmosphere, for example of N_2O and CH_4, the oceanic distribution of these GHGs and the amount exchanged via the air-sea interface is highly variable (Nevison et al., 1995; Holmes et al., 2000; Rhee et al., 2009). Thus, source and sink behaviors of GHGs have been observed on different spatial and temporal scales. In general terms, these behaviors depend on biological and physical processes that promote outgassing or sequestering mechanisms. Physical and biological features of the Southern Ocean suggest the existence of a potential for both the production and removal of CH_4 and N_2O (Rees et al., 1999; Tilbrook and Karl, 1994), although very little information on dissolved N_2O and CH_4 distributions is currently available for the region. The substantial spatial variation in regional gas exchange could be due to the increased gas solubility in low-temperature Subantarctic waters, combined with either the downwelling associated with intermediate and deep water formation in the Northern and Southern part, respectively, of the Antarctic Zone. Additional further variation may be caused by the upwelling of deep and intermediate waters in the southern part of the Polar Frontal Zone (Park and Vivier, 2012).

In different regions of the Southern Ocean, the surface layer is permanently supersaturated with CH_4 (Bates et al. 1996; Tilbrook and Karl, 1994, Toshida et al., 2011), but this is not the case for N_2O, which may occur in either under- or super saturated conditions Law and Ling, 2001, Rees et al., 1997, Zhan and Chen, 2009). Aside from physical processes affecting GHG concentrations in the water column and their concomitant air-sea fluxes, the concentrations also depend on organic matter (OM) availability and oxygen levels, which determines whether aerobic or anaerobic respiration occurs (Codispoti et al., 2001; Reeburgh, 2007). The availability of dissolved iron (dFe) should also be included as a direct variable affecting the recycling of GHG´s (through production and consumption), as several Fe-containing enzymes are required for GHG cycling, which are involved in the electron transfer chains in bacterial respiratory systems and Nitrogen cycling (Arrieta et al., 2004; Kirchman et al., 2003; Morel et al., 2003a). Indirectly, dFe stimulates ocean productivity which can enhance carbon and nitrogen export from the euphotic zone to the subsurface (Boyd and Ellwood, 2010), resulting in a an increase in microbial activities and mediate GHG production via nitrification (Fuhrman and Capone , 1991).

N_2O is mainly produced during the first step of nitrification (the aerobic oxidation of NH_4^+ to NO_2^-), and during partial denitrification (the anaerobic reduction of NO_3^-/NO_2^- to N_2O). N_2O can also be consumed by complete denitrification via dissimilatory reduction to N_2 (Codispoti and Cristiensen, 1985), or assimilatory N_2O reduction to NH_4^+ (Farias et al., 2013). CH_4, on the other hand, is mainly formed by methanogens during anaerobic OM degradation (Wuebble & Hayboe, 2001) or by methylotrophs during CH_4 formation derived from transformations of methyl-compounds such as methylphosphonate (MPn) (Karl et al., 2008), dimethyl-sulphoniopropionate (DMSP) (Damm et al., 2010), and dimethylsulphide (DMS) (Florez-Leiva et al., 2013). In addition, CH_4 can be consumed (oxidized) via aerobic methanothophy (Hanson and Hanson, 1996). Since Southern Ocean waters are well oxygenated, it is thought that the dominant mechanisms of production in surface waters are by either through N_2O formation by nitrification (Nevison et al., 2003) and CH_4 formation via either methanogenesis in suspended particles (Scranton and Brewer, 1977) or methylotrophy (Sun et al., 2011).

The main objective of the present study is to describe for first time the N_2O and CH_4 contents in the Southern Ocean under the influence of natural fertilization during the spring phytoplankton bloom in the Kerguelen Plateau Region (KPR). The determination of the role of the Southern Ocean in CH_4 and N_2O air–sea exchange may be critical in understanding the factors that influence GHG cycling. This includes dFe which comes from different sources within the KPR, inducing mesotrophic conditions associated with the coastal waters of Kerguelen Island and of the central Kerguelen plateau, an area of within the Central Plateau area of the KPR that demonstrates an annually recurrent phytoplanktonic bloom in the (Blain et al., 2008; Chever et al., 2010), and with the Antarctic Polar front and other mesoscale structures (Mongin et al., 2008, Lasbleiz et al., 2014).

2. **Methods**

2.1. Study area

Samples were collected within the Kerguelen Plateau Region or KPR (Fig. 1) during the KEOPS 2 cruise at stations along TNS (46°–51°S) and (TEW (66°–75°E). The cruise took place from October 11th to December 11th, 2011, on board the research vessel (RV) *Marion-Dufresne*. Some of the stations were located in the naturally Fe-enriched PFZ, in the coastal shelf waters of Kerguelen Island and within the southeastern KPR bloom (including station A3 from the previous KEOPS 1 cruise). St. R-2 located east of the Kerguelen plateau was considered to be typical of HNLC conditions (see Table 1). The positions of the stations were selected according to a strategy based on real-time ocean color and altimetry satellite images (d´Ovidio et al., 2015).

2.2. Sampling: Continuous vertical profiles of temperature, salinity, dissolved O_2, fluorescence and Photosynthetically Active Radiation (PAR) were obtained using a conductivity temperature and depth (CTD) sensor. Seawater samples were collected using a SeaBird SBE 911plus CTD unit mounted on a 24 12 L bottles rosette. Water samples for gases (N_2O, CH_4), nutrients, and pigments (sampled in this consecutive order) were obtained from nine depths distributed between the surface and 500 m depth. Water samples for CH_4 (triplicate) and N_2O (triplicate) analyses were taken in 20 mL glass vials and poisoned with $HgCl_2$ (0.1 ml of saturated $HgCl_2$ solution per vial). Subsequently, the vials were sealed with a butyl-rubber septum and an aluminum cap, avoiding bubble formation, and stored in darkness at room temperature until laboratory analysis. Syringes of 50 mL were directly connected to the spigot of the Niskin bottles to take nutrient samples (NO_3^-, NO_2^- , PO_4^{3-} and $H4SiO_4$) at each sampled depth. Duplicate samples were collected and drawn through a 0.45 μm Uptidisc adapted to the syringe, and then immediately analyzed using an autoanalyzer (more details in Blain et al., 2014). Total chlorophyll-a (*TChl-a*) samples in triplicate were filtered into a 25 mm glass- fiber filter (GF/F), and then immediately frozen (-20ºC). Samples were kept until later analysis by high performance liquid chromatography (HPLC) (more details in Lasbleiz et al., 2014).

2.3. Chemical analysis: N_2O and CH_4 were analyzed by via the generation of a 5 mL ultra-pure Helium headspace into the vial using a gastight syringe, then within the vial the gas and liquid phases were equilibrated at 40°C, following this the gases within the vial were quantified through the use of a gas chromatograph determined by Helium equilibration (5-mL Helium headspace and 15-mL of seawater) at 40°C, finally quantification via chromatography was carried out. N_2O was analyzed in a Varian 3380 Gas Chromatograph using an electron capture detector at 350°C and connected to an autosampler device. CH_4 was analyzed in a Schimadzu 17A gas chromatograph using a flame ionization detector at 250°C through a capillary column GS-Q at an oven temperature of 30º C. A calibration curve was made with four concentrations for N_2O (0.1 ppm, 0.32, 0.5 ppm, and 1 ppm, by Matheson standards) and four concentrations for CH_4 (0.5, 1.78, 2 and 10 ppm, by Matheson standards). Both detectors linearly responded to these concentration ranges. The analytical error for the N_2O and CH_4 analyses was less than 3% and 5% respectively. The ECD and FID detectors lineally responded to these concentration ranges and the analytical error for the N_2O measurements for this study was about 3%. The uncertainty of the measurements was calculated from the standard deviation of the triplicate measurements by depth. Samples with a variation coefficient higher than 10 % were not taken into account for the gas database.

More details regarding the analysis of both gases can be found in Farias et al. (2009). Nutrients were immediately analyzed onboard by standard automated colorimetric methods (Tréguer and LeCorre, 1975) using the continuous flow autoanalyser (Skalar). The precision and detection limit of the method was, respectively, ±50 nM and 20 nM for NO_3-, and ±30 nM and 110 nM for PO_4^{-3-} (more details in Blain et al., 2015). NH_4^+ was measured by fluorometric analysis (Holmes et al., 2000) with a precision of ±50 nM.

2.4. Data analysis: To interpret the vertical variation of N_2O and $CH_{4,}$ and assess how biogeochemical processes may affect their concentrations, the water column was divided into two layers according to density gradient: (1) well-mixed and (2) subsurface from the base of the mixed layer (ML) to 500 m (arbitrary depth used only for comparison proposes). Nutrient inventories for T*Chl-a*, N_2O and CH_4 were calculated by numerical integration of data with linear interpolation at intervals of one meter, based on at least 4-6 sampled depths per layer. Saturation percentages of gases were calculated from the measured CH_4 and N_2O concentrations and those estimated to be in equilibrium with the current gas concentrations in the atmosphere register (NOAA/ESRL program http://www.esrl.noaa.gov/gmd/hats/combined/N2O.html) based on *in situ* temperature and salinity records according to the solubility parameterization of CH_4 (Wiesenburg and Guinasso, 1979) and N_2O (Weiss and Price, 1980). GHG flux through the air-sea interface was determined using the following equation, modified by Wanninkhof (1992):

$$F = kw(T°, salinity) \cdot (C_w - C_a)$$

where *kw* is the transfer velocity from the ML to the atmosphere, as a function of wind speed, temperature and salinity in the ML according to parametrization; C_w is the mean gas concentration in the mixed layer; while C_a is the gas concentration in the mixed layer expected to be in equilibrium with the atmosphere. Since gas transfer velocity is related to wind speed, this was calculated according to the well-known exchange models of Liss and Merlivat (1986) or LM86 and Wanninkhof (1992) or W92, based on the dependence of the transfer velocity on wind speed. Wind speed and direction were obtained from the ship's meteorological station. Wind speed was estimated as a moving seven day average prior to the sampling period in order to smooth out short-term fluctuations and highlight longer-term trends. The mixed layer depth was calculated using a potential density-based criterion, defining the mixed layer depth (ML) as the shallowest depth at which density increased by 0.02 kg m^{-3} from the sea surface value.

Pearson product-moment correlations (rs) were determined for GHG, and T*Chl-a* and nutrient inventories were estimated for both the ML and for the whole water column from the surface to 500 m depth. The threshold value for statistical significance was set as $p < 0.05$. A principal component analysis (PCA) using the empirical orthogonal function (EOF; Emery and Thomson, 1997) was performed to find the co-variability patterns of a number of stations located in spatial gradients in terms of nutrients, gases (O_2, N_2O, and CH_4), T*Chl-a*, and dFe. This analysis excluded the stations from the NS transect as no measurements were recorded (Quéroué et al, 2015). PCA were made with all biogeochemical variables measured in the ML and with these variables obtained in the water column from the surface to a depth of 500 m, in order to detect differences in the vertical structure.

Results

3.1. Oceanographic conditions.

Oceanographic characteristics of the sample stations during the KEOPS 2 cruise are shown in Table 1. Two transects, carried out almost synoptically across and along the KPR (survey region – Fig. 1) were undertaken to establish the position of the main mesoscale structures as fronts (Fig. 2). The Polar Front (PF) crosses the KPR and denotes certain physical structures (i.e. convergence processes) visible throughout temperature and salinity (Park and Vivier, 2012).

Regarding the TEW (66° to 75°E, along 47°S), vertical cross sections of temperature and salinity along with a T-S diagram are illustrated in Fig 2 (a, c, e). Temperature and salinity varied between 2.41° and 3.30°C, and between 33.60 and 34.67, respectively. A weak structure with colder and fresher surface waters was registered in the PF, which crossed these transects twice, at ~71°E (St. TEW-3,-4) and at ~73.5°E (St. TEW-7, -8). Middle stations (Sts. TEW-4, -5 and E) are located in an area with a complex recirculatory system. This is a superficial section inundated by mixed Antarctic surface water (AASW) and coinciding with an area of a PF northward inflexion (Fig. 1). The presence of Subantarctic mode water (SAMW) was observed east of 73.5° E (Sts. TEW-7, -8, Fig. 2f). In addition, a marked variability in subsurface water was observed, attributed to the mixing of water masses; this was particularly strong in TEW within the PF, revealing a vertical mixing process produced by convergence, particularly evident at St. TEW-7 (Fig. 2e). Regarding the TNS (46°-51°S, along ~72°E), Fig. 2 (b, d, f) shows vertical cross sections of temperature, salinity and a T-S diagram, respectively. Temperature and salinity fluctuated from 1.67° to 4.17°C and from 33.67 to 34.68, respectively, and a gradual decrease in temperature and an increase in salinity were observed in the surface layer from north to south (Fig 2 b, d). A water parcel of a relatively cold water mass was observed to be spreading northward in subsurface waters. This is noted as an expression of the PF, which marks the location where the AASW moves northward, descends rapidly, and sinks below 200 m depth (Fig. 2 b). These distributions coincided with the expected water mass distribution, this being the case for the northern (Sts. TNS-1,-2) and southern (Sts. A3, TNS-10) stations, mainly occupied from the surface to 250 m by the SAMW and the AASW, respectively (Fig 2f).

3.2. Biogeochemical variables

Figure 3 shows vertical cross sections along the TEW of biogeochemical variables including nutrients (only NO_3^- and PO_4^{3-}), T*Chl-a*, O_2 and GHGs. The surface layer continuously showed NO_3^- concentrations, fluctuating from 22 to 27 µmol L^{-1} (typical condition of the AASW). However, a relative depletion of NO_3^- was observed at the stations located north and eastward of the PF (Fig 3a). PO_4^{3-} presented the same pattern as NO_3^- and the N:P ratio of dissolved nutrients averaged around 14.5, with the exception of some values of 13.2 from stations located close to the PF (Fig. 3 b). *TChl-a* fluctuated from 0.005 to 4.69 µg L^{-1} and peaked at Sts. TEW-1, -2 (both located in a coastal area 10 and 75 km away from Hillsborough Bay coast) and Sts. TEW-7,-8 (to the north of PF). *TChl-a* showed a relative decrease at stations located in the Central Section (Fig. 3c). O_2 concentration varied form 320 µM (in surface water) to 185 µM (at 500 m depth), consistently maintaining super saturation conditions (Fig 3d).

N_2O fluctuated from 14.0 to 25.4 nmol L^{-1} (equivalent to a range of 102-182.2% saturation, Fig 3e). Superficially, in the western and central section (70.5- 73°E) the N_2O concentration was close to equilibrium with the atmosphere in surface waters, and in surface waters at sites where the PF crosses the transect, i.e. Sts. TEW-4 and TEW-7 (Fig. 3e) N_2O was slightly undersaturated (around 90%). N_2O levels increased slightly attaining around 120% saturation towards the subsurface water. CH_4 ranged from 1.4 to 31.35 nmol L^{-1}, equivalent to a saturation range of 43-969%. In contrast to N_2O, surface waters were always supersaturated in CH_4, demonstrating the greatest increase in gas levels (up to

970%) in coastal waters close to Kerguelen Island, a relative decrease (<200% saturation) in the central section (between 71° and 73. Seasonal and inter-annual variability of biogeochemical variables, including nitrous oxide (N_2O) an important climate active gas, were analyzed during monthly observations between 2002 and 2012 at the COPAS Ocean Time-Series station in the coastal upwelling area off central Chile (36° 30.8' S). Oxygen, N_2O, nutrients and chlorophyll-a (T*Chl*-a) showed clear seasonal variability associated with upwelling favorable winds (spring-summer), and also inter-annual variability, which in the case of N_2O was clearly observed during N_2O hotspot occurrence with saturation levels of up to 4849%. The hotspots consistently occurred during the upwelling-favorable period in years 2004, 2006, 2008, 2010 and 2011, below to the mixed layer (15-50 m depth) in waters with hypoxia and specific NO_2^- accumulation. They displayed a 3 times greater apparent N_2O production (ΔN_2O) than the average monthly anomalies (2002-2012). Estimated relationships of ΔN_2O vs. apparent oxygen utilization (AOU) and ΔN_2O vs. NO_3^- suggest that aerobic ammonium oxidation (AAO) and partial denitrification are the processes responsible for high N_2O accumulation in subsurface water. T*Chl*-a levels correlated fairly well with the presence of the N_2O hotspots, suggesting that microbial activities, facilitated by a higher availability of organic substrates, trigger high N_2O levels. This in turn results in a huge efflux into the atmosphere of up to 260 µmol m^{-2} d^{-1}. N_2O hotspots are transient events or hot moments, which may occur more frequently than they are observed. If so, this upwelling area is producing and emitting greater than expected amounts of N_2O and resulting in an important source of N_2O that should be considered in the global atmospheric N_2O balance. 5°S, or Sts. TEW-4, -5 and E2), and a strong increase (up to 778%) at St. TEW-7. Remarkably, CH_4 concentrations in subsurface waters were low compared to the surface waters (Fig. 3f).

Vertical cross sections of biogeochemical variables along the TNS are shown in Figure 4. NO_3^- and PO_4^{3-} gradually increased from north to south from 24 to 30 µmol L^{-1} and from 1.5 to 2 µmol L^{-1}, respectively (Fig 4 a, b). This spatial trend coincided with the expected transition of water mass dominance and its mixing between the SAMW and the AASW (Fig 2 f). T*Chl-a* ranged from 0.005 to 2.391 µg L^{-1} and peaked in the southernmost stations (Sts. TNS-8, -9 and A3-2; Fig. 4b) and coincided with a slight increase in nutrients. There a deep Fe-enriched and lithogenic silica reservoir seemed to influence the area (Lasbleiz et al., 2014; Quéroué et al., 2015). O_2 distribution was similar to that observed in the WE transect.

N_2O concentrations ranged from 12.37 to 23.8 nmol L^{-1}, equivalent to 88.5% to 171% saturation. N_2O levels close to equilibrium or undersaturation were often observed in surface waters, except at St. TNS08 (Fig. 4e). CH_4 varied from 1.47 to 21.88 nM, or 45 to 666% saturation, and peaked in southern stations (Fig 4f). Notably, high levels of T*Chl-a* were associated with high concentrations of CH_4 in this transect. Southern stations had extremely low N_2O concentrations (less than 6.9 nM or 70% saturation), such as St. A3, which is located in an area of relatively high dFe availability and within a phytoplankton bloom.

PCA, including dFe and GHG data were obtained from the TEW as shown in Figure 5. The results did not change when O_2 was removed from the analysis, indicating that O_2 availability does not modify the percentage of the variance. When the data set used in the PCA is restricted to the ML (Fig. 5a), stations located on the TEW were grouped into three sets, clearly separating stations located in eastern (north of the PF, St. TEW-7), western, and coastal areas (TEW-1,-2), and within the central section (Sts. TEW-4, -5, E2). The variability among stations can be predominantly explained by the first component, accounting for 75.7% of the variance. Figure 5 suggests possible interpretations of the relationships between the variables with their respective weights assigned to each of them (illustrated with an eigenvector). The figure shows a close relationship between N_2O, nutrients, CH_4, dFe and T*Chl-a*. The

PCA analysis using data from the entire water column and provided a similar grouping of the sample stations (Fig 5b).

3.3. Vertical distribution of gases and other variables at selected stations

Figure 6 shows typical profiles of oceanographic and biogeochemical variables (including gases). Stations were separated *a priori* according to biogeochemical (PCA analysis for the case of the TEW; Fig.5) and oceanographic criteria (T-S diagram, Fig. 2e, f). Selected stations included: Sts. A3, with a recurrent annual bloom (historical station sampled in KEOPS 1, Blain et al., 2007) and moderate dFe levels (~ 0.18 nmol L^{-1}). Some stations displayed evidence of an active uptake of dFe; St. TEW-7 had one of the highest dFe (~0.40 nmol L-1) and T*Chl-a* levels, and also showed evidence of rapid dFe uptake (Fourquez et. 2014). For comparative purpose, we include the most northern station of the TNS (St. TNS01), St. R-2 (in the HNLC area), and a coastal station close to Kerguelen Island, which had the highest dFe levels (up to 3.82 nmol L^{-1}). Vertical distribution of N_2O and CH_4 clearly varied, while elevated CH_4 concentrations were generally observed superficially and in the ML base, and concentrations decreased with increased depth, whereas N_2O concentrations gradually increased with depth. Gas contents also differed between stations and were observed to correlate in a similar way with with T*Chl-a* and dFe levels.

The stations located at the extremities of the TEW (i.e., TEW-1 and TEW-7) had the highest CH_4 levels (Fig 6), while N_2O levels were relatively low. Conversely, Sts. TNS-1 and A3-2 located in the extreme north and south of the TNS presented relatively low levels of CH_4 compared to the TEW. Station R-2, which is located in the HNLC area had the lowest N_2O and CH_4 content, and both gases were homogeneously distributed with depth (Fig. 6). This is consistent with T*Chl-a* levels of less than 0.5 µg L^{-1}**.**

3.4. Nutrient, T*Chl-a,* dFe and GHG inventories and air-sea GHG exchanges

Table 2 shows the inventories of NO_3, PO_4^{3-} and GHGs in the ML and the water column from the surface to 500 m; mean GHG concentrations in the ML, wind speed, and air-sea GHG fluxes are also included. ML depths varied widely from 16 m (at the station near Kerguelen Island) to 181 m. The T*Chl-a* pool, estimated on the basis of the photic layer, fluctuated from 8.77 to 75.45 mg m^{-2}. Levels were notably elevated at Sts. SPF and A3-2 (up to fivefold greater), in comparison to the more oligotrophic stations such as St. R-2. Surface NO_3^- and PO_4^{3-} inventories did not show significant differences among stations and varied between 1.56 to 16.03 and 0.13 to 1.07 mol m^{-2}, respectively. Minimal values were registered at stations St. TEW-7--8 and TNS-1, both located north of the PF.

N_2O pools varied from 0.201 to 2.55 and from 1.12 to 10.05 mmol m^{-2} in the ML and the whole water column, respectively. Minimum values were registered in the ML at stations within the PF and also to the north. These surface pools did not significantly correlate with T*Chl-a*, but correlated strongly and negatively with nutrients (rs: 0.91 $p<0.001$ for NO_3^- and rs: 0.92, $p<0.001$ for PO_4^{3-}). CH_4 inventories fluctuated between 0.19 and 3.31 mmol m^{-2} for the ML, and 1.06 and 7.44 mmol m^{-2} for the whole water columns. Once again, inventories in the ML were two and fivefold higher at Sts. TEW-7 and A3-2, respectively, than at St. R-2. CH_4 inventories were four and sevenfold higher in Sts. TEW-7 and A3-2, respectively, than at St. R-2. The comparison between the CH_4 inventories (standardized by the thickness of the layer) obtained from the ML and from the entire water column indicates that the maximum values came from the ML's base, remarkably in the PF (Table 2). CH_4 pools correlated positively with T*Chl-a* pools (rs= 0.69; $p<0.05$), but did not show any correlation with NO_3^- and PO_4^{3-}. Thus, minimum values for both nutrients were found when T*Chl-a* was higher.

Average hourly wind velocity during the cruise was 10.53 ±5.52 m s^{-1}, occasionally falling below 0.31 m s^{-1} or rising above 29.1 m s^{-1}. The ML depth did not show any significant relationship to wind speed (rs: 0.20 p=0.41) or the water mass structure (Table 1 and Fig. 2), but seems to be related to the complex mesoscale circulation observed in the KPR (Park et al., 2014; Zhou et al., 2014). N_2O fluxes, estimated by LM86, fluctuated between -9.69 and 10.02 μmol m^{-2} d^{-1} (mean: 1.25±4.04 μmol m^{-2} d^{-1}), while those estimated by W92 varied from -18.69 to 20.2 μmol m^{-2} d^{-1} (mean: 2.41±7.88). Substantial differences were observed between the cubic (LM86) and the quadratic parameterizations (W92) during high wind speeds; such as those measured during the N-S transect (21-23 October 2011, mean value of 12.08 m s^{-1}), compared to those registered during the TEW (31 October – 02 November, mean value of 5.61 m s^{-1}). The W92 increased in calculated fluxes by approximately a factor of two at high wind speeds, while at low wind speeds the difference between LM86 and W92 was up to a factor of ~1.6 (see Table 2). CH_4 fluxes varied from 0.21 to 38.1 μmol m^{-2} d^{-1} (mean: 10.01±9.97), and from 0.32 to 70.24 μmol m^{-2} d^{-1} (mean: 21.27±21.07), when LM86 and W92 were employed, respectively. At times the study area acted as a source of very high CH_4 effluxes into the atmosphere, particularly at stations St. TNS-9 and St. A3-2 where emissions were around three times as high as those calculated for St. R-2. There are important differences between the two parameterizations, although the same trend was obtained among stations (Table 2).

4. Discussion

Iron fertilization in the KPR influences phytoplankton growth and primary production (PP), and other microbial activities (Cavagna et al., 2014; Christaki et al., 2014), as well as relative CH_4 accumulation (Fig. 3f and Fig. 4f) and some N_2O depletion (Fig 3e). The gas distribution pattern clearly matched those of Queroue et al. (2014) for T*Chl-a* and PCA grouped stations using dFe. The segregation of stations includes; the coastal area (Sts. TEW-1, -2), the PF (St. STEW-7) and the central plateau region (Sts. A3-2). In the case of KEOPS 2, phytoplanktonic blooms were mainly represented by a microplanktonic community (Lasbeiz et al., 2014), as those observed in the north Polar Front (St. TEW-7) and the central part of the KPR (A3) stations displayed high rates of iron uptake (Quéroué et al., 2014). These previously indicated areas, demonstrated variable but high particulate Fe of biogenic origin (Van der merwe et al., 2015). This confirms an increased biological uptake which in turn determines a rapid dFe turnover. The observed gas distribution patterns raise questions as to how the complex circulation and some mesoscale structures support relatively high T*Chl-a* accumulation and microbial activities in comparison to surrounding waters, and particularly whether there are some fertilization mechanisms (including the addition of Fe and nutrients) promotes GHG cycling and its associated microbial activities.

4.1. N_2O cycling

Fuhrman and Capone (1991) pointed out the stimulation of ocean productivity through the addition of Fe enhances nitrogen export from the euphotic zone to the subsurface layer and may result in enhanced N_2O formation via the stimulation of nitrification. This stimulation may occur through the activation of metallo-proteins that are involved in the various stages of ammonium and nitrite oxidation, as ammonia oxidizing nitrifiers oxidize NH_4^+ and NH_2OH to NO_2^- using iron-containing ammonia monooxygenase (AMO) and hydroxylamine oxidoreductase (HAO), respectively (Morel et al., 2003b). Since N_2O is a powerful greenhouse gas, 300 times more radiative than CO_2 per molecule, Fe addition could counteract the climatic benefits of atmospheric CO_2 drawdown (Jain et al., 2000). The link between Fe fertilization and enhanced N_2O formation via nitrification was supported by Law and Ling (2001), who found a small but significant N_2O accumulation in the pycnocline during the Southern Ocean Iron Enrichment Experiment (SOIREE) at 61°S, 140°E. Jin and Gruber (2003) subsequently predicted the long-term effect of Fe fertilization on global oceanic N_2O emissions using a coupled physical-biogeochemical model. Based on the model outputs, it was concluded that Fe fertilization induced N_2O emissions that could offset the radiative benefits of the CO_2 drawdown. However, during other Southern Ocean Iron

Enrichment Experiments (EIFEX), Walter et al. (2005) found no N_2O enrichment after artificial Fe fertilization.

Our findings revealed that natural Fe fertilization did not appear to stimulate N_2O accumulation in the superficial layer (within the ML). There was no significant difference in the N_2O inventory estimates from areas of higher accumulation of biomass with respect to those estimated for St. R-2, which was used as a reference station (Table 2). Contrary to what was expected, no increase in N_2O content was observed at stations close to Kerguelen Island (St TEW-1, TEW-2), which are highly enriched by dFe from fresh water and sediments (Quéroué et al., 2014). This trend suggests that nitrifiers in surface water are not being significantly stimulated by dFe supply from the sediments. In subsurface water (below ML to 500 m depth) N_2O accumulation may be associated with nitrification and it is noted that dual nitrate isotopic composition ($\delta^{15}N\text{-}NO_3^-$ and $\delta^{18}O\text{-} NO_3^-$) revealed an increase in both isotope values with greater water depth in subsurface waters (100–400 m). This is a result of the partial consumption of available nitrate in surface waters, the export of low $\delta^{15}N$ in Particulate Nitrogen (NP) and the remineralization–nitrification that occurs in this situation (Dehairs et al., 2014). However, values of $\delta^{15}N\text{-}NO_3^-$ and $\delta^{18}O\text{-} NO_3^-$ in surface waters also suggests that nitrification is also occurring in surface waters, but with a considerable variation.

Notably, the St. TEW-7, -8 and A3-2 were observed to be in equilibrium and slightly depleted in N_2O (Fig. 3e; Table 2). It is likely that the explanation for this would be that the mixing process produced at the PF (St. TEW-7) (with moderate levels of Fe, high levels of T*Chl-a*, and evidence of active Fe uptake) may stimulate the N fixers, as demonstrated by Mills et al. (2004), Berman-Frank et al. (2007), and Moore et al. (2009). N-fixing microorganisms may have an effect on the N_2O inventory as they could be used as an alternate substrate for fixers, as suggested by Farias et al. (2013). Thus, biological N_2O fixation could be using and assimilating N_2O, producing N_2O depletion and a simultaneous undersaturation. N-fixation has been observed in the cold waters of the Arctic and Antarctic (Blais et al., 2012; Diez et al., 2012, Diez unpublished data), as well as in cold upwelled water (Fernandez et al., 2011), suggesting that N_2O fixation may also occur more commonly than originally expected. Coincidently, St. TEW-7 (within the PF) also had the highest surface N-fixation (Gonzalez et al., 2014), suggesting that N_2O is used as a substrate by diazotrophs (Farias et al., 2013) and that this process is stimulated by enhanced Fe supply. N_2O undersaturation or equilibrium with the atmosphere was observed in the TNS (Fig, 4e), particularly at stations north of the PF with influence from the SAMW. This suggests that some kind of process occurring that removes or consumes gas from the upper water column. A notable level of undersaturation was also observed at St. A3-2, which is located in the recurring phytoplankton bloom and within a system of relatively high dFe concentration due to the presence of the Plateau (Blain et al., 2007).

N_2O undersaturation has been reported, although rarely, in Polar and Sub-polar Ocean regions (Butler et al., 1989; Law and Ling, 2001; Foster et al., 2009). Physical processes related with gas solubility and deviations from the atmospheric equilibrium gas concentration could not explain the observed undersaturation. It is probable that if the physical variables alter faster than that expected for gas equilibrium with the atmosphere that there may be a gas deficit. Thus, deviation from the equilibrium condition could be caused by rapid heating or cooling, refreshing, and/or a mixing of water masses (Sarmiento and Gruber, 2006). An analysis of these potential changes was made for the AASW and the SAMW. A cooling (decreasing T°C> 3) or fresh water influence (decreasing S from 34 to 10) would be required to produce the observed undersaturation, neither of which was observed during the sampling (Table 1), or expected during this season (Park et al., 2014). Additionally, if the two water masses were mixed proportionally, as they are, the resulting process cannot produce undersaturation in regards to the original N_2O levels and the signature temperature and salinity. Recently, Chen et al. (2014) reported that surface water of the Indian sector of the Southern Ocean were understaturated in N_2O, suggesting a N_2O influx. This phenomenon in the surface water may result from the intrusion of freshwater from ice melt and the northeastward transport of the AASW. However, in the KPR, N_2O undersaturation seems to be located in an area of high particle concentration under the influence of the SAMW (northern the PF), Thus, a preliminary analysis indicates that biological processes are responsible for the N_2O undersaturation and the concomitant influx from the atmosphere. In contrast, subsurface waters have higher N_2O concentrations (saturations from 120% to 180%) than surface waters, which indicate a net accumulation. In this case the most likely process responsible for N_2O accumulation is aerobic ammonium oxidation (Codispoti et al., 2001), but no significant difference was noted at the stations with the highest T*Chl-a* levels, indicating that N_2O production by nitrification was not substantially stimulated at those stations.

4.2. CH_4 cycling

There have been few studies on CH_4 distribution and production in the Southern Ocean (Lamontage et al., 1973; Tilbrook and Karl, 1994; Heeschen et al., 2004). Surface water in the Southern Ocean has been reported to be undersaturated or lightly saturated with respect to atmospheric CH_4, as a result from the entrainment of CH_4 depleted deep water into surface water and from the seasonal ice covers acting as a barrier for gas exchange (Toshida et al., 2011). Regarding the effect of iron addition on CH_4 cycling, Wingenter et al. (2004) found low levels of CH_4 production (less than 1%) during artificial Southern Ocean Fe enrichment experiments (SOFex). Simulated large-scale Southern Ocean Fe fertilization (OIF) also resulted in anoxic conditions which may favor anaerobic methanogenesis (Oschlies et al., 2010). However, our results show that surface and subsurface waters are supersaturated in CH_4 with a fourfold enrichment in CH_4 with respect to the control area (Fig. 3e), this was associated to areas with elevated T*Chl-a* levels and iron uptake by microbial communities (Fourquez et al., 2014). Results showed a marked spatial differences in CH_4 content measured in the TEW and TNS (t-student: 3.21 $p<0.001$) (Fig. 3f and 4f), and that surface CH_4 accumulation generally coincided with areas of relatively higher dFe levels, which in turn favors primary production (PP). Likewise, the CH_4 accumulation at pycnoclines (Fig. 6) indicates that most CH_4 came from accumulated particles sinking from the surface water, as commonly observed by Holmes et al. (2000) in different marine systems. The PCA analysis, which included the measurement of dFe revealed a close relationship between CH_4 accumulation and Fe availability and clearly grouped in areas with different biogeochemical characteristics. The fact that the western and eastern sections showed high Fe levels (Quéroué et al., 2014,) relative to the Central Section of the W-E transect, and that these sections had high CH_4 levels, which suggests that Fe stimulates CH_4 production. A similar situation occurs in Sts.A3 with high T*Chl-a* levels and PP rates, as shown by Cavagna et al. (2014). For example, station A3-2 and TEW-7 (maximum T*Chl-a*) had the highest integrated primary production rates (up to 3380 mg m^{-2} d^{-1}) and the lowest C export level of around 2-3% (Cavagna et al., 2014), this suggests an intense level of PP supported by regenerated N sources. These contrast with the observed situation at St. R-2 with the lowest rate of regenerated production (with a PP rate of around 135 mg m^{-3} d^{-1} and an exported C rate of around 25% of PP).

Two hypotheses exist for CH_4 production in surface waters; One is that production only occurs in association with anoxic particles (Karl and Tilbrook, 1994), produced for the most part by grazing zooplankton, as methanogenic bacteria were considered to be present in an anaerobic microenvironment in organic particles (pellets) or in the guts of zooplankton (Alldredge and Cohen, 1987; Karl and Tilbrook, 1994). The other hypothesis was formulated more recently, that phytoplankton blooms should favor zooplankton grazing process and/or stimulate bacterioplankton activity as CH_4 is generated via the degradation of organic methyl compounds by bacteria (Karl et al., 2008).

Increased grazing of microbes by microzooplankton, as observed by Christaki et al. (2014), may contribute to particle recycling (rich in organic carbon and DMSP), and increase the potential for methanogenesis (Weller et al., 2013). Yoshida et al. (2011) found that high CH_4 production in the Southern Ocean probably resulted from the grazing processes of Antarctic krill and/or from zooplankton that feed on phytoplankton, and the subsequent microbial methanogenesis. This agrees with the findings of sites enriched with iron and biomass that exhibit high carbon fluxes at 100 m depth, dominated by large fecal pellets rather than phytodetrital aggregates (Laurenceau-Cornet et al., 2015).

Conversely, aerobic CH_4 production in the water column could be associated with heterotrophic activities (2015) showed that the highest bacterial production rates (up to 110 mg C m^{-2} d^{-1}), and the greatest abundance of heterotrophic bacteria were associated with stations where the phytoplankton bloom was developed (TEW-7 and A3-2). Recent evidence indicates that methylotrophs are candidates for mediated CH_4 generation using methylated compounds as DMSP and DMS (Florez-Leiva et al., 2013; Weller et al., 2013). Among these heterotrophic microorganisms DMS degradation can be ascribed to methylotrophic bacteria (Visshser et al., 1994) that derives energy from the conversion of methyl into other products, as well as using S as a source for methionine biosynthesis (Kiene et al., 1999). Current studies of natural and cultivated SAR11 alphaproteobacteria (strain Ca. P. ubique HTCC1062; Sun et al., 2011) indicate that these microorganisms, among the most abundant heterotrophic bacteria in surface waters, possess genes that are encoded for oxidation pathways of a variety of one-carbon compounds, and have the capacity for demethylation and C1 oxidation, but do not incorporate C1 compounds as biomass. This suggests that there is a close relationship between phytoplankton, the only producers of DMSP (Yoch, 2002), and microbial communities which may be recycling DMS. Phyto- and bacterioplankton relationships control DMS turnover, which could result in several mechanisms of DMSP/DMS degradation (Simó et al., 2002; Vila-Costa et al., 2006) and produce

CH_4 (Damm et al., 2010; Florez-Leiva et al., 2013; Weller et al., 2013). These publications show that phytoplankton species composition and biomass in different bloom phases, as well as eddy dynamics, were important determinants of CH_4 saturation and emission.

With regards to the distribution, vertical profiles of the gas indicate that most CH_4 is being formed at the surface and at pycnoclines (at the base of the ML), and consumed at subsurface and intermediary depths (Figure 6). Thus, CH_4 distribution appears to be controlled largely by biological mechanisms rather than by mixing, contrary to what has been reported by Heeschen et al. (2004). In general, surface waters of the Southern Ocean were undersaturated with respect to atmospheric CH_4 as the result of the entrainment of CH_4 depleted deep water to the surface and from seasonal ice cover acting as a barrier for gas exchange. We observed CH_4 undersaturation, fluctuating between 40% and 90%, at most sampled stations at depths of > 200. It is unlikely that this undersaturation results from the entrainment of CH_4 depleted waters that have high levels of gas solubility, but instead by a biological consumption as it is more likely that a biological mechanism is involved. The only known process able to consume CH_4 is methanotrophy, and the fact that subsurface waters were depleted of CH_4 suggests that CH_4 consumption is higher than production, or that no production occurs in subsurface waters. Interestingly, although CH_4 microbial oxidation occurs throughout the water column and is recognized as an important process that reduces CH_4 emissions (Reeburgh et al., 2007; Rehder et al., 1999), there have been few investigations on microbial communities mediating aerobic CH_4 oxidation. There does exist a few measurements of aerobic CH_4 oxidation in marine environments, and measurements taken from open systems under oligotrophic regimes (Tilbrook and Karl, 1994, Holmes et al., 2000) which report lower levels of oxidation than in the oxic/anoxic interface (Sansone and Martens, 1978 Reeburgh et al., 1991).

4.3. CH_4 and N_2O emission in the southern Ocean

Highly dynamic gas exchanges were registered in the KPR, with source and sink scenarios for N_2O and only a source scenario for CH_4. Since the mean wind speed did not exceed 14 m s^{-1}, LM86 and W92 parameterizations represent the more conservative overestimation estimates of gas exchange in the area (Frost and Upstill-Goddard, 2003). The gas inventories in the ML reflect the effect of gas transport mainly via turbulent mixing and advection, which can be accelerated by the action of wind but also by the microbial activity in surface waters. The ML depth did not correlate to wind speed (rs: 0.31, $p < 0.05$) and this aids to estimate the gases content in the ML and whether it is a result of in situ production or consumption. CH_4 fluxes were higher at stations located at the PF and A3, where phytoplanktonic blooms were observed (see Table 2), but the tendency was the reverse for N_2O, with an influx into the aforementioned stations. CH_4 emission rates during this study were higher than previously measured (Table 2), with a range of 0.1 to 3.0 μmol m^{-2} d^{-1} for the Pacific Ocean (Bates et al., 1996; Holmes et al., 2000; Sansone et al., 2001) and 0.5 to 9.7 μmol m^{-2} d^{-1} for the Atlantic Ocean (Oudot et al., 2002; Forster et al., 2009). In the South Pacific ocean (10°-64°S, 140°E), crossing the PF, Yoshida et al. (2011) reported CH_4 fluxes ranging from 2.4 to 4.9 μmol m^{-2} d^{-1}.

In the case of N_2O, the estimates in this study were in the expected range for the oligotrophic open ocean (Nevison et al., 1995). N_2O undersaturation and the concomitant influx were estimated, although this situation has not yet been well described for the Southern Ocean. N_2O sinks can occasionally be observed (Butler et al., 1989; Law and Ling, 2001) which can be explained by probable N_2O assimilation by N-fixing microorganisms. This process may be responsible for the estimated N_2O influx.

5. Implications

The dynamics of both gases differ substantially both spatially and vertically (surface to 500 m depth), indicating that different mechanisms are being activated to produce an active gas during recycling. Our findings also show that in areas of active fertilization and biogenic particle accumulation, CH_4 accumulates while N_2O becomes depleted. This study suggests that the Antarctic Polar Zone plays a significant role in surface CH_4 production and subsequent air-sea gas exchange. These results did not agree with some previous studies of artificial fertilization experiments in the Southern Ocean, although only a few studies of this nature exist. This indicates that the turnover and evolution of microbial communities in mesoscale structures are fundamental for the development of substrates and conditions for CH_4 regeneration. Surface N_2O does not spatially respond to natural iron fertilization, at least in terms of N_2O production via nitrification or that N_2O consumption does not occur any rapider than the N_2O production process. However in subsurface water N_2O accumulation seems to take place via nitrification.

Acknowledgements: We would like to thank the captain and crew of the R/V Marion Dufresne. We recognized the support of both project leaders (Stephane Blain and Bernard Queguiner). This work was supported by the French Research program of INSU-CNRS LEFE−CYBER (Les enveloppes fluides et l'environnement –Cycles biogéochimiques, environnement et ressources), the French ANR (Agence Nationale de la Recherche, SIMI-6 program, ANR-10-BLAN-0614), the French CNES (Centre National d'Etudes Spatiales) and the French Polar Institute IPEV (Institut Polaire Paul−Emile Victor).We are also grateful to Louise Oriol and Stephane Blain for nutrient data and Marine Lasbleiz for the HPLC analysis of chlorophyll measurements. The altimeter and colour/temperature products for the Kerguelen area were produced by Ssalto/Duacs and CLS with support from Cnes. We also recognize all our colleagues that contributed to KEOPS 2. CF and LF were supported by the Proyecto Ecos-Conicyt C09B02 and the International Associated Laboratory MORFUN. CF received partial support from Fondap N°15110027. LF founded the analysis of samples obtained in the KEOPS 2 cruise with FONDECYT N° 1120719. This is a contribution by 15110009 (FONDAP-CONICYT).

References

Alldredge, A. L. and Y.Cohen. Can microscale chemical patches persist in the sea? Microelectrode study of marine snow, fecal pellets, Science, 235, 689–691, doi:10.1126/science.235.4789.689, 1987.

Arrieta, J.M., Weinbauer, M.G., Lute, C. and Hernd, G.J. Response of bacterioplankton to iron fertilization in the Southern Ocean, Limnology and Oceanography, 49(3), 799-808, 2004.

Bates T.B., Kelly, K.C., Johnson, J.E. and Gammon, R.H. A re-evaluation of the open ocean source of methane to the atmosphere, Journal of Geophysical Research, 101 (D3), 6953–6961, 1996.

Berman-Frank, I., Quigg, A., Finkel Z. V., Irwin A.J., Haramaty, L. Nitrogen-fixation strategies and Fe requirements in cyanobacteria, Limnology and Oceanography, 52(5), 2260–2269, 2007.

Blain, S., Quéguiner, B., Armand, L., Belviso, S., Bombled, B., Bopp, L.,Bowie, A., Brunet, C., Brussaard, K., Carlotti, F., Christaki, U., Corbiére, A., Durand, I., Ebersbach, F., Fuda, J.L., Garcia, N., Gerringa, L.J.A., Griffiths, F.B., Guigue, C., Guillerm, C., Jacquet, S., Jeandel, C., Laan, P., Lefe`vre, D., Lomonaco, C., Malits, A., Mosseri, J., Obernosterer, I., Park, Y.H., Picheral, M., Pondaven, P., Remenyi, T., Sandroni, V., Sarthou, G., Savoye, N., Scouarnec, L., Souhault, M., Thuillers, D., Timmermans, K.R., Trull, T., Uitz, J., Van-Beek, P., Veldhuis, M.J.W., Vincent, D., Viollier, E., Vong, L and Wagener, T. Effect of natural iron fertilization on carbon sequestration in the Southern Ocean, Nature, 446 (7139), 1070–1075, 2007.

Blain, S., Sarthou, G. and Laan, P. Distribution of dissolved iron during the natural iron fertilization experiment KEOPS (Kerguelen Plateau, Southern Ocean), Deep-Sea Research II, doi:10.1016/ j.dsr2.2007.12.028, 2008.

Blain, S., Capparos, J., Guéneuguès, A., Obernosterer, I. and Oriol, L. Distributions and stoichiometry of dissolved nitrogen and phosphorus in the iron fertilized region near Kerguelen (Southern Ocean). Biogeosciences, 12, 623-635, 2015. doi:10.5194/bg-11-5931-2014

Blais, M.,Tremblay J.-É., Jungblut, A. D., Gagnon, J., Martin, J., Thaler, M. and Lovejoy, C. Nitrogen fixation and identification of potential diazotrophs in the Canadian Arctic. Global Biogeochemical Cycles, 26, GB3022, doi:10.1029/2011GB004096, 2012

Butler, J. H.,Elkins, J.W., Thompson, T. M and Egan. K.B. Tropospheric and Dissolved N_2O of the West Pacific and East Indian Oceans During the El Niño Southern Oscillation Event of 1987, Journal of Geophysical Research, 94, 14865-14877, 1989.

Cavagna, A.J., Lefèvre, D., Dehairs, F., Elskens, M., Fripiat, F., Closset, I., Laslbleiz, M., Florez-Leiva, L., Cardinal,D., Leblanc, K. , Fernandez, C., Oriol, L., Blain, S. and Quéguiner, B. Biological productivity regime and associated N cycling in the vicinity of Kerguelen Island area, Southern Ocean . Biogeosciences Discuss., 11, 18073-18104, 2014.

Chen. L., Zhang, J., Zhan, L., Li, Y., Sun, H. Differences in nitrous oxide distribution patterns between the Bering Sea basin and Indian Sector of the Southern Ocean. Acta Oceanologica 33, 9‑19, DOI: 10.1007/s13131-014-0484-8, 2014.

Chever, F., Sarthou, G., Bucciarelli, E., Blain, S. and Bowie, A.R.. An iron budget during the natural iron fertilisation experiment KEOPS (Kerguelen Islands, Southern Ocean). Biogeosciences, 7: 455-468, 2010.

Christaki, U., Lefèvre, D, Georges, C., Colombet, J., Catala, P., Courties, C., Sime-Ngando, T., Blain, S. and Obernosterer, I. Microbial food web dynamics during spring phytoplankton blooms in the naturally iron-fertilized Kerguelen area (Southern Ocean). Biogeosciences, 11, 6739-6753, 2014.

Cicerone, R.J. and Oremland, R.S. Biogeochemical aspects of atmospheric methane, Global Biogeochemical Cycles, 2, 299–327, 1988.

Codispoti, L.A and Christensen, J.P. Nitrification, denitrification and nitrous oxide cycling in the eastern Tropical South Pacific Ocean, Marine Chemistry, 16, 277-300, 1985.

Codispoti, L. A., Brandes, J. A. Christensen, J. P. Devol, A.H. Naqvi, S.W.A., Paerl, H.and Yoshinari, T. The oceanic fixed nitrogen and nitrous oxide budgets: Moving targets as we enter the anthropocene?, Scientia Marina, 65, 85-105, 2001.

Damm, E., Helmke, E., Thoms, S., Schauer, U., Nöthing, E., Bakker, K., Kiene, R.P. Methane production in aerobic oligotrophic surface water in the central Artic ocean, Biogeosciences, 7, 1099-1108, 2010.

Dehairs, F, Fripiat, F., Cavagna A.-J. Trull, T. W. Fernandez, C., Davies, D. Roukaerts A., Fonseca Batista, D. Planchon, F. and Elskens M. Nitrogen cycling in the Southern Ocean Kerguelen Plateau area: evidence for significant surface nitrification from nitrate isotopic compositions. Biogeosciences Discussion, 11, 13905-13955, 2014

Díez, B., Bergman, B., Pedrós-Alió, C., Antó, M. and Snoeijs P. High cyanobacterial nifH gene diversity in Arctic seawater and sea ice brine. Environmental Microbiology Reports 4, 360–366, doi:10.1111/j.1758-2229.2012.00343.x, 2012.

d'Ovidio, F., Della Penna, A., Trull, T.W., Nencioli, F., Pujol I., Rio, M. H., Park Y.-H. , Cotté C., Zhou, M. and Blain S.The biogeochemical structuring role of horizontal stirring: Lagrangian perspectives on iron delivery downstream of the Kerguelen plateau. Biogeosciences Discuss., 12, 779-814, 2015.

Emery, W.J and Thomson, R.E. Data analysis methods in physical oceanography, Pergamon Press, 634 pp, 1997.

Farias, L., Fernández, C., Faúndez, J., Cornejo, M. and Alcaman, M.E. Chemolithoautotrophic production mediating the cycling of the greenhouses gases N_2O and CH_4 in an upwelling ecosystem, Biogeosciences, 6, 3053-3069, 2009.

Farias, L., Faundez, J., Fernadez, C., Cornejo, M., Sanhueza, S and Carrasco, C. Biological N_2O fixation in the eastern South Pacific ocean, PLoS One 8, e63956, doi:10.1371 /journal.pome0063956, 2013.

Florez-Leiva, L., Damm, E. and Farías, L. Methane production induced by methylsulfide in surface water of an upwelling ecosystem, Progress in Oceanography, doi.org/10.1016/ j.pocean. 2013.03.005, 2013.

Fourquez, M., Obernosterer, I., Davies, D.M., Trull, T.W and Blain, S. Microbial iron uptake in the naturally fertilized waters in the vicinity of Kerguelen Islands: phytoplankton-bacteria interactions. Biogeosciences Discuss., 11, 15053-15086, 2014.

Frost, T., and Upstill-Goddard, R.C. Meteorological controls of gas exchange at a small English lake, Limnology and Oceanography, 47(4), 2002, 1165–1174, 2002.

Forster, G., Upstill-Goddard, R.C., Gist, N., Robinson, C., Uher, G.,Woodward, E.M. Nitrous oxide and methane in the Atlantic Ocean between 50°N and 52°S: Latitudinal distribution and sea--air flux, Deep-Sea Research II 56, 964-976, 2009.

Fuhrman, J.A. and Capone, D.G. Possible biogeochemical consequences of ocean fertilization, Limnology and Oceanography, 36, 1951-1959, 1991.

Grasshoff, J. Methods of seawater analysis. In: Grasshoff K, Ehrhardt M, Kremling K (eds.). Methods of seawater analysis Verlag chimie Germany, 1983.

Gonzalez, M.L., Molina, V., Florez-Leiva, L. Cavagna, A.J., Dehairs, F., Farias, L. and Fernandez, C. Nitrogen fixation in the southern ocean: A case of study of the Fe-fertilized Kerguelen region (KEOPS II cruise). Biogeosciences Discuss., 11, 17151-17185, 2014

Hanson, R.S. and Hanson, T.E. Methanotrophic bacteria, Microbiology and Molecular Biology Reviews, 60(2), 439-471, 1996.

Heeschen, U. K., Keir, R. S., Rehder, G., Klatt, O and Suess, E. Methane dynamics in the Weddel Sea determined via stable isotope ratios and CFC‐11, Global Biogeochemical. Cycles, 18, GB2012, doi:10.1029/2003GB002151, 2004, Holmes, R.H., Aminot, A., Kérouel, R., Hooker, B.A., Peterson, J. A simple and precise method for measuring ammonium in marine and freshwater ecosystems. Canadian Fisheries and Aquatic Sciences, 56,1801-1808, 1999.

Holmes, M.E., Sansone, F.J., Rust, T.M. and Popp, B.N. Methane production, consumption, and air-sea exchange in the open ocean: An evaluation based on carbon isotopic ratios, Global Biogeochemical Cycles, 14, 1 – 10, 2000.

IPCC, 2013: Climate Change 2013: The Physical Science Basis. Contribution of Working Group I to the Fifth Assessment Report of the Intergovernmental Panel on Climate Change Stocker, T.F., D. Qin, G.-K. Plattner, M. Tignor, S.K. Allen, J. Boschung, A. Nauels, Y. Xia, V. Bex and P.M. Midgley (eds.). Cambridge University Press, Cambridge, United Kingdom and New York, NY, USA, 1535 pp.

Jain, A. K., Briegleb, B.P., Minschwaner, K. and Wuebbles D. J. Radiative forcing and global warming potentials of greenhouse gases, Journal Geophysical Research, 105, 20,773–20,790., 2000.

Jin, X. and Gruber, N. Offsetting the radiative benefit of ocean iron fertilization by enhancing N_2O emissions. Journal Geophysical Research, 30,, 2249, doi:10.1029/2003GL018458, 2003.

Jouandet, M-P., Jackson, G. A., Carlotti, F., Picheral, M.,Stemmann, L. and Blain, S. Rapid formation of large aggregates during the spring bloom of Kerguelen Island: observations and model comparisons Biogeosciences Discussion., 11, 4949–4993, doi:10.5194/bgd-11-4949-2014, 2014.

Karl, D.M., Tilbrook, B.D. Production and transport of methane in oceanic particulate matter, Nature, 368, 732–734, 1994.

Karl, D., Beversdorf, L., Björkman, K.M., Church, M.J., Martinez, A., DeLong, E.F. Aerobic production of methane in the sea, Nature Geoscience, 1, 473-478, 2008.

Kiene, R.P. Linn, L.J. J. Gonzalez,J. M.A. Moran, M.A Bruton, J.A. Dimethylsulfoniopropionate and methanethiol are important precursors of methionine and protein-sulfur in marine bacterioplankton. Applied and Environmental Microbiology, 65 (10), 4549–4558, 1999.

Kirchman, D.I, Hoffman, K.A. Weaver, R. and Hutchins, D.A. Regulation of growth and energetics of a marine bacterium by nitrogen source and iron availability, Marine Ecology Progress Series, 250, 291-296, 2003.

Lamontagne, R., Swinnerton, J. W., Linnenbom, V.J. and Smith, W. D. Methane concentrations in various marine environments. Journal of Geophysical Research, 78, 5317-5324, 1973.

Laurenceau-Cornet, E.C., Trull, T. W., Davies, D. M., Bray, S. G., Doran, J., Planchon F., Carlotti, F., Jouandet, M.-P., Cavagna, A.-J. , Waite, A. M. and Blain S. The relative importance of phytoplankton aggregates and zooplankton fecal pellets to carbon export: insights from free-drifting sediment trap deployments in naturally iron-fertilised waters near the Kerguelen plateau. Biogeosciences, 12, 1007–1027, 2015

Law, C. and Ling, R. Nitrous oxide flux and response to increased iron availability in the Antarctic Circumpolar Current, Deep Sea Research Part II: Topical Studies in Oceanography, 48, 2509-2527, 2001.

Lasbleiz, M., Leblanc, K., Blain, S., Ras, J., Cornet-Barthaux, V., Nunige, S.H. and Quéguiner, B., 2014a. Pigments, elemental composition (C, N, P, Si) and stoichiometry of particulate matter, in the naturally iron fertilized region of Kerguelen in the Southern Ocean. Biogeosciences, 11: 5931–5995, doi:10.5194/bg-11- 5931-2014, 2014

Liss P.S, Merlivat L. Air-sea gas exchange rates: Introduction and synthesis. In: Buat-Menard P. (ed.), The Role of Air-Sea Exchange in Geochemical Cycling. D. Reidel, Dordrecht, pp. 113-127, 1986.

Nevison, C., Weiss, R. and Erickson III, D.J. Global oceanic emissions of nitrous oxide, Journal of Geophysical Research, 100, 15809-15820,1995.

Nevison, C., Butler, J.H. and Elkins, J.W. Global distribution of N_2O and the DN2O-AOU yield in the subsurface ocean, Global Biogeochemical Cycles, 7 (4), 1119, doi:10.1029/2003GB002068, 2003.

Mills, M.M.,Ridame, C., Davey, M., La Roche, J and Geider, R. Iron and phosphorus co-limit nitrogen fixation in the eastern tropical North Atlantic, Nature., 429, 292–294, 2004.

Mongin, M., Molina, E. and Trull, T. Seasonality and scale of the Kerguelen plateau phytoplankton bloom: A remote sensing and modeling analysis of the influence of natural iron fertilization in the Southern Ocean, Deep Sea Research Part II: Topical Studies in Oceanography, 55(5-7), 880-892, 2008.

Moore, C.M , Mills, M.M., Achterberg, E.P., Geider., R J. LaRoche, J., Lucas, MI., McDonagh, E.L., Pan, X., Poulton, A.J., Rijkenberg, M J. A., Suggett, D.J., Ussher, S. J. and Woodward, E.M.S. Large-scale distribution of Atlantic nitrogen fixation controlled by iron availability, Nature Geoscience, 2, 867–871, 2009.

Morel, F.M.M. and Price, N.M. The biogeochemical cycles of trace metals in the Oceans, Science, 300, 944, DOI: 10.1126/science.1083545, 2003a.

Morel, F. M. M., Milligan, A.J. and Saito M.A. Marine Bioinorganic Chemistry: The Role of Trace of Metals in the Oceanic Cycles of Major Nutrients in *Treatise on Geochemistry*, Vol. 6, edited by KK. Turekian, H.D. Holland, Elsevier Science Ltd, Cambridge, UK, p. 113-143, 2003b

Oudot, C., Jean-Baptiste, P., E. Fourreb, E. Mormichea, C. Guevela, M., Ternonc, J.-F , Le Corred, P. Transatlantic equatorial distribution of nitrous oxide and methane, Deep-Sea Research I, 49,1175–1193, 2002.

Oschlies, A., W. Koeve W., Rickels W., and Rehdanz, K. Side effects and accounting aspects of hypothetical large-scale Southern Ocean iron fertilization, Biogeosciences 7, 4017–4035, 2010.

Park, Y-H and Vivier, F. Circulation and hydrography over the Kerguelen Plateau. Marine ecosystems and fisheries, 5, 43-55, 2012.

Park, Y.-H., Durand, I., Kestenare, E., Rougier, G., Zhou, M., d'Ovidio, F., Cotté, C. and Lee, J.-H. Polar Front around the Kerguelen Islands: An up-to-date determination and associated circulation of surface/subsurface waters. Journal Geophysical Research- Oceans, 119: doi:10.1002/2014JC010061, 2014.

Quéroué, F., Sarthou, G., Chever, F., Van der Merwe, P., Lannuzel, D., Townsend, A.,Bucciarelli, E, Planquette, H., Cheize, M., Blain, d'Ovidio, F. and A. Bowie, A. A new study of natural Fe fertilization processes in the 2 vicinity of the Kerguelen Islands (KEOPS 2 experiment), KEOPS 2 Biogeoscience discussion 12, 231-279, 2015.

Rees, A.P., Owens, N.J.P and Upstill-Goddard, R.C. Nitrous oxide in the Bellingshausen Sea and Drake Passage, Journal of Geophysical Research,102, 3383– 3391, 1999.

Reeburgh, W.S, Ward, B.B, Whalen, S.C., Sandbeck, K.A., Kilpatrick, L.J and Kerkhof, K. Black Sea methane geochemistry, Deep-Sea Research II (38) S1189–S1210, 1991.

Reeburgh, W.S. Oceanic methane biogeochemistry. Chemical Reviews 107, 486–513, 2007.

Rehder, G., Keir, R.S., Suess, E., Rhein, M. Methane in the northern Atlantic controlled by microbial oxidation and atmospheric history, Geophysical Research Letters 26, 587–590, 1999.

Rhee, T. S., Kettle, A. J and Andreae, M. O. Methane and nitrous oxide emissions from the ocean: A reassessment using basin-wide observations in the Atlantic, Journal of Geophysical Research, 114,D12304, doi:10.1029/2008JD011662, 2009.

Sanial, V., van Beek, P., Lansard, B., Souhaut, M., Kestenare, E., and d'Ovidio, F., Zhou, M. and Blain, S. Radium isotopes to track sediments-derived inputs of the Kerguelen Plateau, Biogeosciences, Biogeosciences Discuss, 11, 14023-14061, 2014

Sansone F.J. and Martens, C.S. Methane oxidation in Cape Lookout Bight, North Carolina, Limnology and Oceanography, 23, 349–355, 1978.

Sansone, F.J., Popp, B.N., Gasc, A. Graham, W. Rust, T.M. Highly elevated methane in the eastern tropical North Pacific and associated isotopically enriched fluxes to the atmosphere, Geophysical Research Letters, 28 4567–4570, 2001.

Sarmiento, J.L. and Gruber, N. Ocean Biogeochemical Dynamics. Princeton University Press, 2006.

Scranton, M.I and Brewer, P. Occurrence of methane in the near-surface waters of the western subtropical North Atlantic, Deep-Sea Research, 24, 127-138, 1977.

Simó, R., Archer, S.D., Pedró-Alió, C., Gilpin, L., Stelfox-Widdicombe, C.E. Coupled dynamics of dimethyl- sulfoniopropionate and dimethylsulfide cycling and the microbial food web in surface waters of the North Atlantic, Limnology and Oceanography, 47, 53–61, 2002.

Sun, J., Steindler, L. J. Thrash, C. , Halsey, K.H., Smith, D.P. Amy E. Carter, A.E. , Zachary C. Landry,Stephen J. Giovannoni. One Carbon Metabolism in SAR11 Pelagic Marine Bacteria. PloS one DOI: 10.1371/journal.pone.0023973, 2011.

Tilbrook, E.D and Karl, D.M. Dissolved methane distributions, sources, and sinks in the western Bransfield Strait, Antarctica, Journal of Geophysical Research, 99, 16383–16393, 1994.

Tréguer P, Le Corre P Manuel d'analyse des sels nutritifs dans I'eau de mer Utilisation de 1'AutoAnalyzt-r 2 Technicon, 2nd edn. 'Univ Bretagne occidentale, Brest, 1975.

Turner, S.M., Harvey, M. J., Law, C. S., Nightingale, P.D and Liss P.S. Iron-induced changes in oceanic sulfur biogeochemistry, Geophysical Research Letter, 31, L14307, doi:10.1029/2004GL020296, 2004.

Van der merwe, P., Bowie, A.R., Quéroué, F., Armand, L., Blain, S., Chever, F., Davies, D., Dehairs, F., Planchon, F., Sarthou, G. et al., 2014. Sourcing the iron in the naturally-fertilised bloom around the Kerguelen Plateau: particulate trace metal dynamics. Biogeosciences, 12, 739-755, 2015

Vila-Costa, M., Simó, R., Harada, H., Gasol, J.M., Slezak D. and Kiene, R.P. Dimethylsulfoniopropinate uptake by marine phytoplankton, Science, 314, 652, 2006.

Vissher, P.T. ,Kiene, R.P., Taylor B.F. Demethylation and cleavage of demethylsulfoniopropionate in marine intertidal sediments, FEMS Microbiology Ecology, 14 179–190, 1994.

Walter, S., Peeken, I., Lochte, K and Bange, H.W. Nitrous oxide measurements during EIFEX, the European Iron Fertilisation Experiment in the subpolar South Atlantic Ocean, Geophysical Research Letter, 32, L23613,doi: 10.1029/2005GL024619, 2005.

Wingenter, O.W., Haase, K.B., Strutton, P., Friedrich, G., Meinardi, S., Blake, D.R and Rowland, F. S. Changing concentrations of CO, CH_4, C_5H8, CH_3Bt, CH_3I and dimethyl sulfide during the Southern Ocean Iron Enrichment Experiments, Proceedings of the National Academy of Sciences101, 8537–8541, 2004.

Wanninkhof, R. Relationship between wind speed and gas exchange over the ocean, Journal Geophysical Research, 97, 7373-7382, 1992.

Weisenburg, D.A and Guinasso, N.L. Equilibrium solubilities of methane, carbon monoxide and hydrogen in water and seawater, Journal of Chemical Engineering Data, 24, 354-360, 1979.

Weiss, R.F. and Prince, B. A. Nitrous oxide solubility in water and seawater, Marine Chemistry 8, 347-359, 1980.

Weller D.I ., Law, C.S., A. Marriner, A., Nodder S.D., Chang, F.H., Stephens, J.A., Wilhelm S.W., Boyd P.W., Sutton P.J.H. Temporal variation of dissolved methane in a subtropical mesoscale eddy during a phytoplankton bloom in the southwest Pacific Ocean, Progress in Oceanography., 116, 193–206, 2013.

Wolfe, R.S. Microbial formation of methane, Advance Microbial Physiology, 6, 107–146, 1971.

Wuebbles, D.J and Hayhoe, K. Atmospheric methane and global change, Earth-Science Reviews, 57, 177–210, 2002.

Yoch, D. Dimethylsulfoniopropionate: Its Sources, Role in the Marine Food Web, and Biological Degradation to Dimethylsulfide Applied Environmental Microbiology 2002; 68(12), 5804–5815, 2002. doi: 10.1128/AEM.68.12.5804-5815, 2002.

Yoshida, O., Inoue, H. Y., Watanabe, S, Suzuki, K. and Noriki, S. Dissolved methane distribution in the South Pacific and the Southern Ocean in austral summer J. Geophysical Research 116, C07008, 2011, doi:10.1029/2009JC006089, 2011.

Zhou, M., Zhu, Y., d'Ovidio, F., Park, Y.-H., Durand, I., Kestenare, E., Sanial, V., Van-Beek, P., Queguiner, B., Carlotti, F., and Blain, S.: Surface currents and upwelling in Kerguelen Plateau regions, Biogeosciences Discussion, 11, 6845–6876, 2014.

Figure caption

Figure 1. Map showing the location of biogeochemical stations sampled during the KEOPS 2 cruise. Bathymetric topography is shown in the main oceanographic region. The orange line delimits the position of the polar front. The transects are indicated.

Figure 2. Left column: a) Temperature (T°C), c) Salinity and e) T-S diagram for E-W transect. Station located close to the PF (purple) is shown, showing enhanced water mass mixing. Arrows indicate position of PF crossing this transect. Right column: b) Temperature (T°C), d) Salinity and f) T-S diagram for the TEW .

Figure 3. Vertical cross section of a) nitrate (µmol L^{-1}); b) phosphate (µmol L^{-1}); c) chlorophyll-a (µg L^{-1}); d) dissolved oxygen (µmol L^{-1}), e) nitrous oxide (nmol L^{-1}) and f) methane (nmol L^{-1}) for zonal transect between 69-75°E. Arrows indicate position of PF crossing this transect

Figure 4. Vertical cross section of a) nitrate (µmol L^{-1}); b) phosphate (µmol L^{-1}); c) chlorophyll-a (µg L^{-1}); d) dissolved oxygen (µmol L^{-1}), e) nitrous oxide (nmol L^{-1}); f) methane (nmol L^{-1}) for the meridional transect between 45°-51°S.

Figure 5. PCA analysis with environmental data including dissolved iron obtained in the zonal transect (TEW). PCA comprises a) data from the surface to the base of the MLand b) environmental data from the surface to 500 m depth. Stations along with the eigenvectors are included.

Figure 6. Vertical distribution of biogeochemical variables from selected stations. Different biogeochemical regimes are defined as HNLC area (St. R), northern and southern area of Polar front (St. TNS-1 and A3-2) and close to the Polar front (Sts. TEW-3 and TEW-7).

Table 1. General oceanographic features of the sampled stations during the KEOPS 2 cruise

Biogeochemical Provinces	**Stations**	**Latitude** °S	**Longitude** °E	**Date** mm-dd-yy	**Bottom Depth (m)**	**MLD (m)**	**Temperature (ºC)**	**Salinity**	**Oxygen (µmol L^{-1})**
	OISO-6	-44.59	52.06	10-15-11	3260	110	3.68 (3.66-3.68)	33.80 (33.80-33.81)	317.4 (314-318)
	OISO-7	-47-4	58.00	10-16-11	4300	127	4.75 (4.73-4.76)	33.79 (33.8-33.81)	308.4 (305-309)
N-S transect									
	A3-1	-50,38	72.05	10-19-11	535	181	1.68 (1.68-1.73)	33.89 (33.85-33.91)	325.9 (321-327)
	A3-2	-50.38	72.05	10-16-11	527	165	2.16 (2.10-2.18)	33.91 (33.911-33.913)	333.2 (329-335)
	TNS10	-50.12	72.07	10-21-11	565	163	1.67 (1.59-1.68)	33.90 (33.80-33.93)	325.9 (314-327)
Eddy	**TNS-9**	-49.47	72.12	10-21-11	615	137	1.75(1.66-1.89)	33.91(33.80-33.84)	321.1 (265-331)
Eddy	**TNS-8**	-49.27	72.14	10-21-11	1030	139	2.11 (2.06-2.12)	33.869 (33.86-33.87)	329.4 (324-328)
	TNS-7	-49.08	72.17	10-22-11	1890	62	2.10 (1.95-2.16)	33.86 (33.86-33.87)	327.7 (327-331)
	TNS-6	-48.48	71.18	10-22-11	1885	67	2.32 (2.23-2.42)	33.846 (33.84-33.85)	327.6 (315-316)
	TNS-5	-48.28	72.12	10-22-11	2060	114	2.22 (2.09-2.26)	33.85 (33.85-33.86)	326.7(323-328)
	TNS-3	-47.05	71.55	10-23-11	540	111	2.17 (2.06-2.26)	33.89(33.88-33.89)	307.6(304-310)
	TNS-2	-47.19	71.42	10-23-11	520	65	3.60 (3.38-3.67)	33.69 (33.68-33.69)	318.6 (317-319)
	TNS-1	-46,.49	71.30	10-23-11	2280	45	4.02(3.96 -4.13)	33.71(33.71-33.72)	316.1 (315-318)
HNLC	**R-2**	-50.21	66.43	10-23-11	2300	111	2.11 (2.06-2.14)	33.78 (33.77-33.78)	326.7 (326-327)
E-W transect									
(Shelf)	**TEW-1**	-49,08	69.50	10-31-11	86	16	3.27 (3.17-3.36)	33.61(33.61-33.62)	344.16 (340-345)
(Shelf)	**TEW-2**	-48,53	70.39	10-31-11	84	40	2.55 (2.49-2.68)	33.75 (33.75-33.76)	332,0 (327-337)
(Shelf)	**TEW-3**	48,47	71.01	10-31-11	565	62	2.17 (2.12-2.31)	33.86 (33.86-33.87)	329.69 (328-331)
	TEW-4	-48,37	71.28	11-01-11	1585	95	2.54 (2.41-2.60)	33.85 (33.85-33.86)	334.60 (331-337)
	TEW-5	48,28	72.47	11-01-11	2275	60	2.51 (2.39-2.60)	33.84 (33.84-33.85)	331.42 (327-336)
(NPF)	**TEW-7**	-48,27	73.59	11-02-11	2510	17	4.02 (3.91-4.10)	33.78 (33.784-33.79)	315.95 (346-349)
	TEW-8	-48,28	75.19	11-02-11	2786	22	4.15 (4.08-4.18)	33.76 (33.76-33.77)	338.75(347-350)
Time Series Stations									
	E-1	-48.27	72.11	10-28-11	2056	84	2.48 (2.36-2.54)	33.85(33.84-33.85)	331.54(328-333)
	E-2	-48.31	72.04	11-01-11	2003	42	2.42 (2.28-2.56)	33.85 (33.85-33.86)	331.68 (329-333)
	E-3	-48.48	71.58	11-03-11	1915	41	2.74 (2.60-2.81)	33.84 (33.84-33.85)	332.08 (331-332)
	E-4W	48.45	71.25	11-11-11	1384	67	2.36 (2.07-2.51)	33.90 (33.90-33.91)	329.95 (326-332)
	E-4E	48.42	72.33	11-12-11	2210	77	3.15 (2.78-3.19)	33.84 (33.83-33.85)	329.89 (326-331)
	E-5	48.24	71.50	11-18-11	1920	36	2.53 (2.50-2.62)	33.85 (33.85-33.85)	326.97(330-333)

Table 2. Inventories of gases and nutrients estimated in the mixed layer (ML) and the entire water column, along with GHG concentrations, wind velocities and concomitant estimated gas exchange across the air-sea interface

Station	**Inventory in the ML**					**Inventory in the Water Column**				**GHGs**		**Wind**	**Flux LM86**		**Flux W92**	
	Chl-a	**CH_4**	**N_2O**	**NO_3^-**	**PO_4^{3-}**	**N_2O**	**CH_4**	**NO_3-**	**PO_4^{3-}**	**N_2O**	**CH_4**		**N_2O**	**CH_4**	**N_2O**	**CH_4**
	mg m^{-2}	**mmol m^{-2}**	**mmol m^{-2}**	**mol m^{-2}**	**mol m^{-2}**	**mmol m^{-2}**	**mmol m^{-2}**	**mol m^{-2}**	**mol m^{-2}**	**nM**	nM	**m s^{-1}**	**µmol m^{-2} d^{-1}**		**µmol m^{-2} d^{-1}**	
N-S Transect																
A3-1	12.60	3.00	2.43	5.41	0.293	5.72	4.12	7.342	0.940	13.73	6.56	6.58	-1.54	18,75	-2.96	35.93
A3-2	35.48	3.31	1.81	4.38	0.300	5.273	3.31	15.04	1.024	11.64	8,,37	11.39	-10.5	14.24	-22.9	29.70
TNS10	14.09	1.39	2.56	4.79	0.319	9.29	2.17	16.03	1.077	15.49	7.79	12.66	3.57	14.90	6.56	27.48
TNS-9	35.58	1.33	2.23	3.91	0.254	7.51	1.87	12.53	0.864	15.89	14.54	14.38	5.08	38.10	9.36	70.26
TNS-8	23.23	0.68	2.16	3.98	0.260	9.27	1.58	15.75	1.038	15.46	5.65	11.89	4.29	7.80	7.92	14.38
TNS-7	25.45	0.25	1.02	1.69	0.111	9.99	1.80	15.74	1.072	16.92	4.01	11.89	8.65	2.03	15.55	3.66
TNS-6	16.33	0.57	0.92	1.83	0.123	8.65	2.54	15.93	1.070	13.81	8.74	11.89	-0.78	17.59	-1.20	31.64
TNS-5	17.19	0.74	1.68	3.07	0.212	9.27	2.46	15.39	1.070	14.67	6.41	11.40	1.81	9.91	3.26	17.82
TNS-3	17.28	0.88	1.75	3.06	0.214	7.75	3.14	12.46	0.875	11.05	7.23	11.40	4.13	9.93	6.85	16.44
TNS-2	11.25	0.26	0.91	1.73	0.123	8.27	1.57	15.08	1.046	13.92	4.38	9.73	1.48	3.03	2.45	5.00
TNS-1	11.21	0.39	0.63	1.07	0.076	8.89	3.16	14.17	0.976	13.95	8.48	9.73	2.26	14.40	3.74	23.84
R-2	14.89	0.64	1.63	2.79	0.197	2.83	1.06	4.900	0.347	14.83	6.29	6.86	0.89	4.09	1.34	6.15
W-E Transect																
TEW-1	9.78	0.19	0.26	3.40	0.412	1.18	1.30	1.560	0.111	15.29	9.50	4.60	0.87	3.15	1.69	6.15
TEW-2	9.87	0.43	0.62	0.84	1.073	1.12	1.74	1.873	0.133	15.03	9.88	4.60	0.54	3.24	1.06	6.33
TEW-3	8.77	0.73	0.91	0.51	1.566	7.41	2.40	14.97	1.072	15.56	14.09	4.60	0.67	5.25	1.32	10.24
E--2	15.33	0.52	0.20	0.82	1.167	9.78	2.80	15.24	1.051	14.95	11.42	6.92	1.34	11.67	2.01	17.57
TEW-4	35.53	0.40	1.63	0.30	2.468	10.3	1.81	15.74	1.106	16.62	3.50	6.92	3.76	0.21	5.67	0.32
TEW-5	23.11	0.38	0.99	0.52	1.619	10.21	2.61	15.62	1.099	16.31	6.35	6.92	3.28	4.34	4.94	6.54
TEW-7	75.45	0.19	0.23	2.39	0.353	9.26	7.44	15.23	1.087	12.90	10.87	8.04	-0.96	15.42	-1.52	23.78
TEW-8	59.52	0.10	0.37	1.52	0.472	10.05	1.59	15.27	1.058	15.77	4.95	8.04	5.25	3.52	8.10	5.42

*Inventories estimated from the photic zone

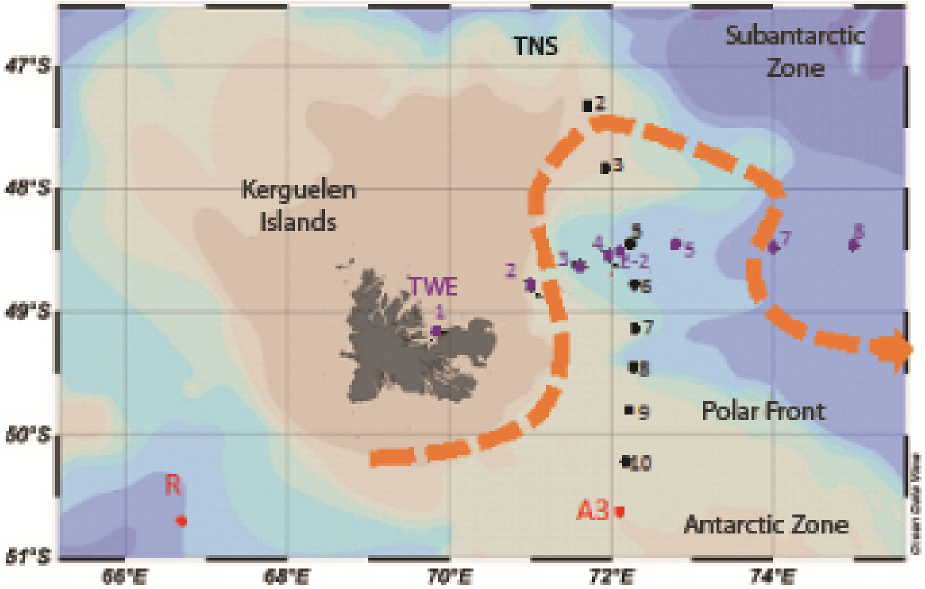
TNS
Subantarctic Zone
47°S
48°S
49°S
50°S
51°S
Kerguelen Islands
TWE
1
2
3
4
5
6
7
8
9
10
E-2
Polar Front
Antarctic Zone
R
A3
66°E
68°E
70°E
72°E
74°E
Ocean Data View

Figure 1

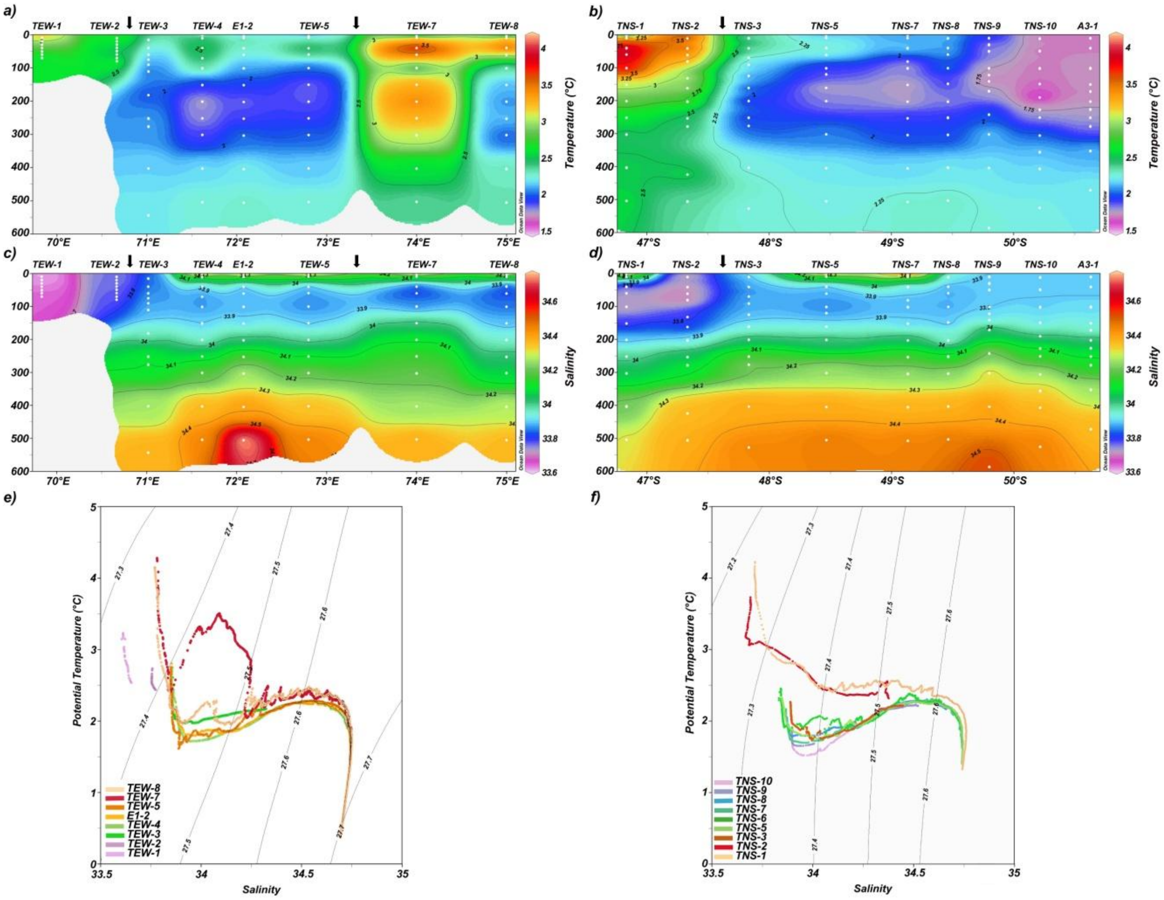
a)
TEW-1
TEW-2
TEW-3
TEW-4
E1-2
TEW-5
TEW-7
TEW-8
70°E
71°E
72°E
73°E
74°E
75°E
Temperature (°C)
b)
TNS-1
TNS-2
TNS-3
TNS-5
TNS-7
TNS-8
TNS-9
TNS-10
A3-1
47°S
48°S
49°S
50°S
c)
Salinity
d)
e)
Potential Temperature (°C)
Salinity
TEW-8
TEW-7
TEW-5
E1-2
TEW-4
TEW-3
TEW-2
TEW-1
f)
TNS-10
TNS-9
TNS-8
TNS-7
TNS-6
TNS-5
TNS-3
TNS-2
TNS-1
33.5
34
34.5
35

Figure 2

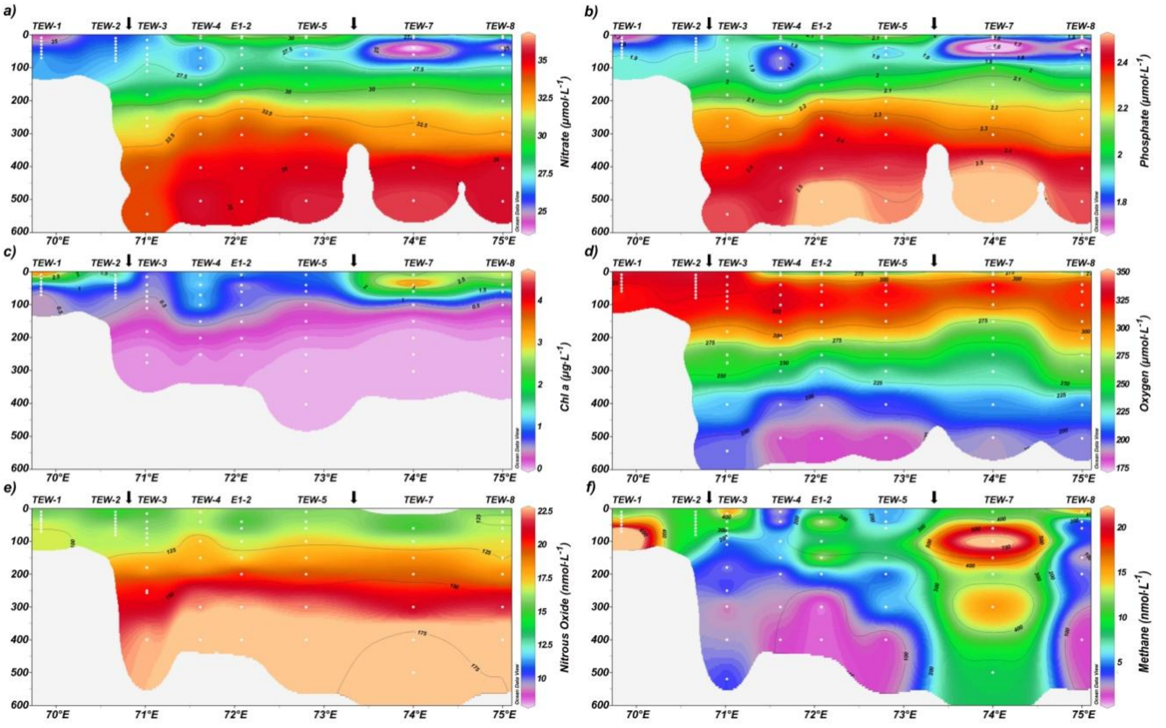

Figure 3

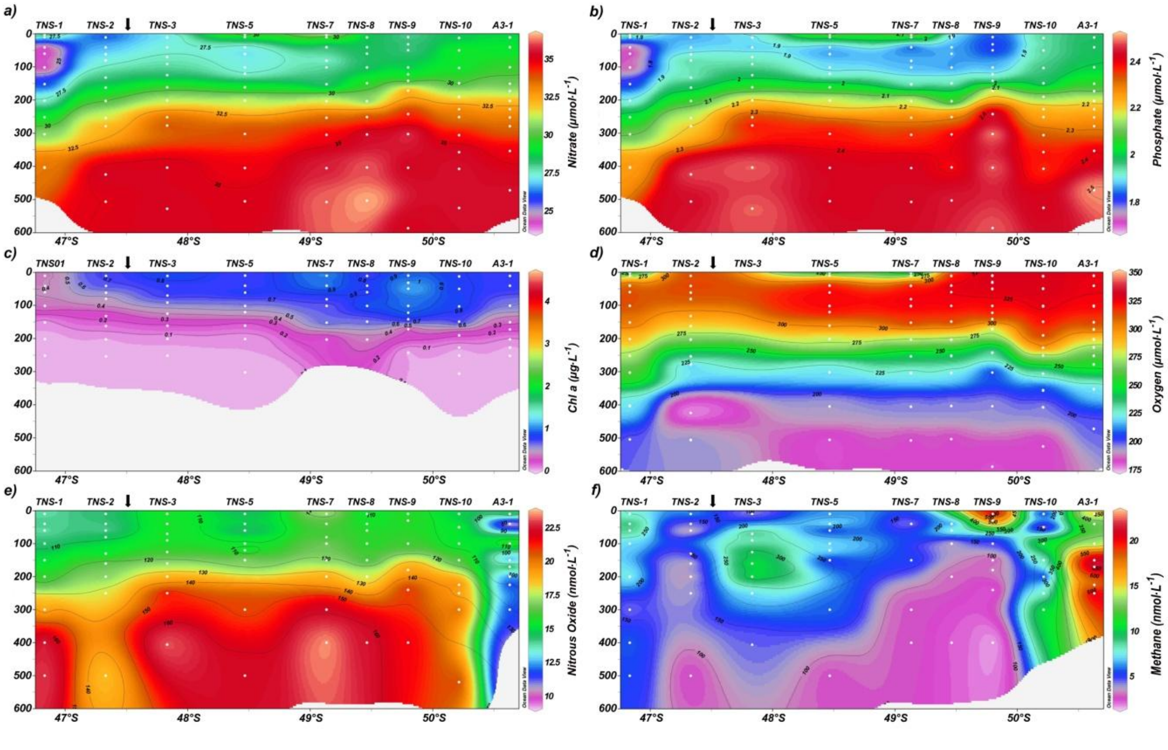

Figure 4

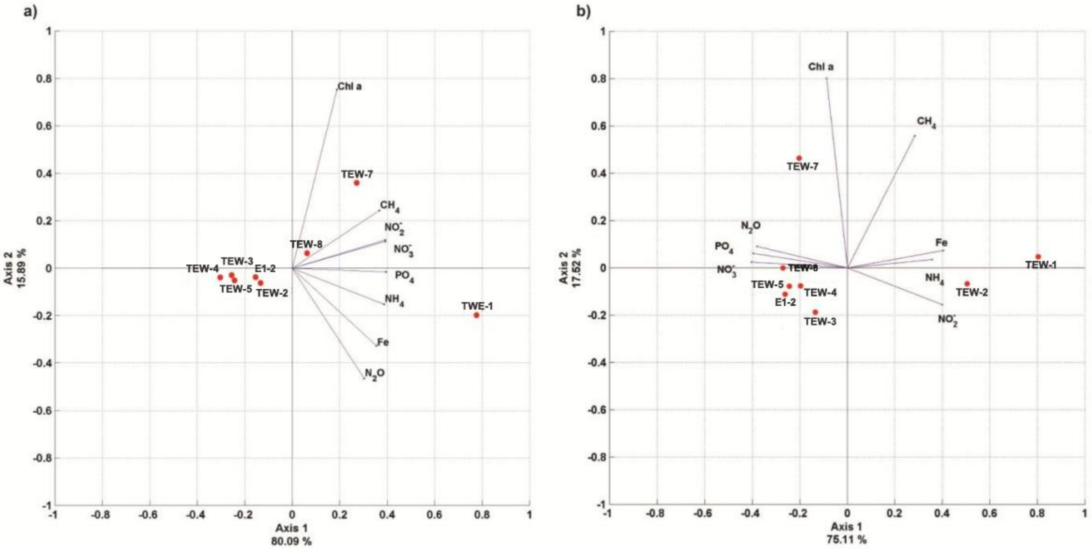
a)
Axis 2
15.89 %
Axis 1
80.09 %
1
0.8
0.6
0.4
0.2
0
-0.2
-0.4
-0.6
-0.8
-1
-1
-0.8
-0.6
-0.4
-0.2
0
0.2
0.4
0.6
0.8
1
Chl a
TEW-7
CH_4
NO_2^-
TEW-8
NO_3^-
TEW-3
TEW-4
E1-2
PO_4
TEW-5
TEW-2
NH_4
TWE-1
Fe
N_2O
b)
Axis 2
17.52 %
Axis 1
75.11 %
1
0.8
0.6
0.4
0.2
0
-0.2
-0.4
-0.6
-0.8
-1
-1
-0.8
-0.6
-0.4
-0.2
0
0.2
0.4
0.6
0.8
1
Chl a
CH_4
TEW-7
N_2O
PO_4
Fe
NO_3^-
TEW-8
TEW-1
NH_4
TEW-5
TEW-4
TEW-2
E1-2
TEW-3
NO_2^-

Figure 5

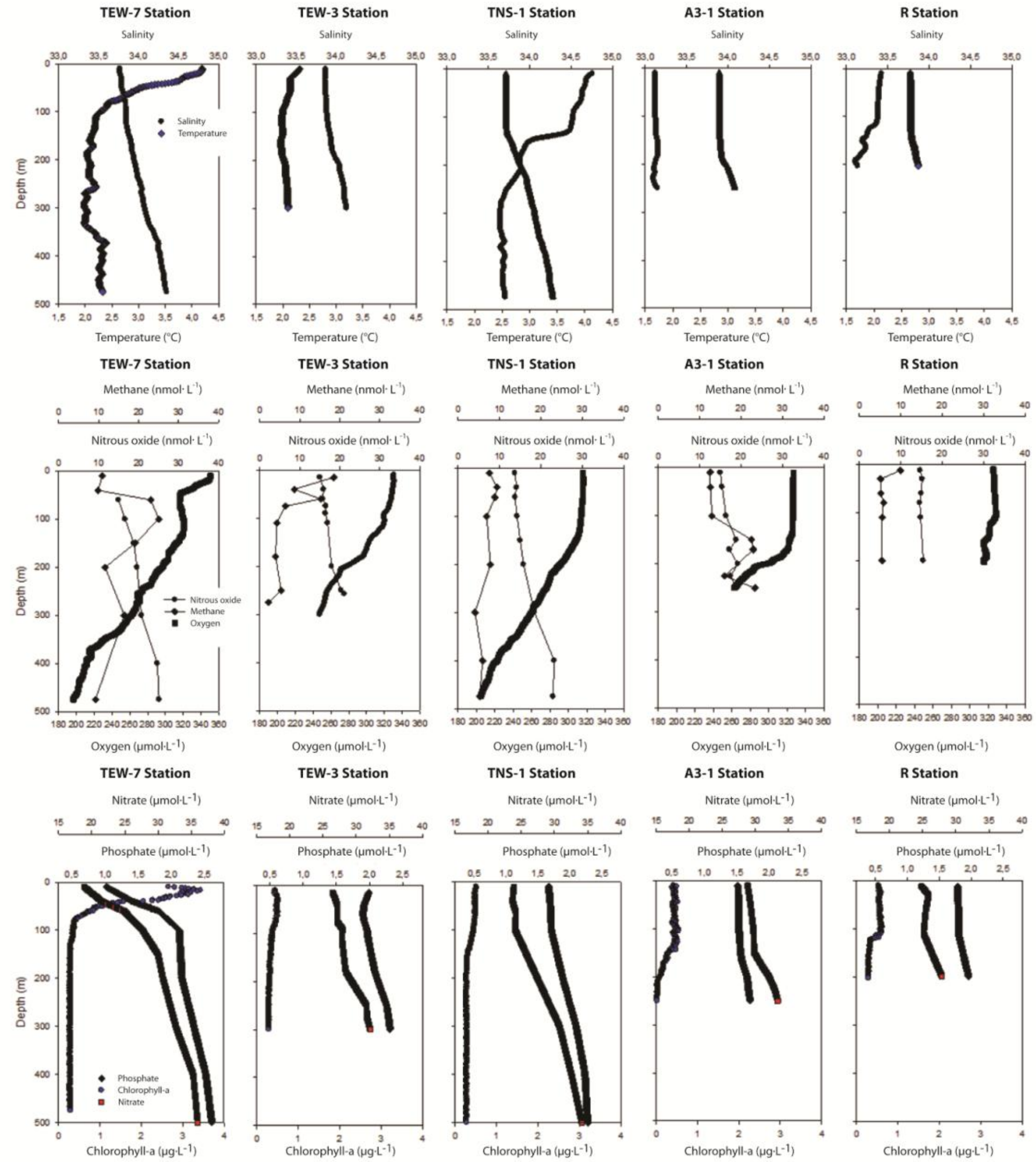
TEW-7 Station
TEW-3 Station
TNS-1 Station
A3-1 Station
R Station
Salinity
33,0 33,5 34,0 34,5 35,0
Temperature (°C)
1,5 2,0 2,5 3,0 3,5 4,0 4,5
Depth (m)
0 100 200 300 400 500
Salinity
Temperature
Methane (nmol· L⁻¹)
0 10 20 30 40
Nitrous oxide (nmol· L⁻¹)
0 10 20 30 40
Oxygen (µmol·L⁻¹)
180 200 220 240 260 280 300 320 340 360
Nitrous oxide
Methane
Oxygen
Nitrate (µmol·L⁻¹)
15 20 25 30 35 40
Phosphate (µmol·L⁻¹)
0,5 1,0 1,5 2,0 2,5
Chlorophyll-a (µg·L⁻¹)
0 1 2 3 4
Phosphate
Chlorophyll-a
Nitrate

Figure 6